Mechanism of the Pseudoirreversible Binding of Amantadine to the M2 Proton Channel

Salomé Llabrés,[†,#] Jordi Juárez-Jiménez,[†,#] Matteo Masetti,[‡] Rosana Leiva,[§] Santiago Vázquez,[§] Sabrina Gazzarrini,[‖] Anna Moroni,[‖] Andrea Cavalli,[*,‡,⊥] and F. Javier Luque[*,†]

[†]Department of Nutrition, Food Science and Gastronomy, Faculty of Pharmacy and Food Sciences, and Institute of Biomedicine (IBUB), University of Barcelona, Avgda. Prat de la Riba 171, 08921 Santa Coloma de Gramenet, Spain

[‡]Department of Pharmacy and Biotecnology (FaBit), Alma Mater Studiorum, University of Bologna, via Belmeloro 6, 40126 Bologna, Italy

[§]Laboratori de Química Farmacèutica (Unitat Associada al CSIC), Facultat de Farmàcia i Ciències de l'Alimentació, and Institute of Biomedicine (IBUB), Universitat de Barcelona, Av. Joan XXIII 27-31, 08028 Barcelona, Spain

[‖]Department of Biosciences and National Research Council (CNR) Biophysics Institute (IBF), University of Milan, Via Celoria 26, 20133 Milan, Italy

[⊥]CompuNet, Istituto Italiano di Tecnologia (IIT), via Morego 30, 16163 Genova, Italy

S Supporting Information

ABSTRACT: The M2 proton channel of influenza A virus is an integral membrane protein involved in the acidification of the viral interior, a step necessary for the release of the viral genetic material and replication of new virions. The aim of this study is to explore the mechanism of drug (un)binding to the M2 channel in order to gain insight into the structural and energetic features relevant for the development of novel inhibitors. To this end, we have investigated the binding of amantadine (Amt) to the wild type (wt) M2 channel and its V27A variant using multiple independent molecular dynamics simulations, exploratory conventional metadynamics, and multiple-walkers well-tempered metadynamics calculations. The results allow us to propose a sequential mechanism for the (un)binding of Amt to the wt M2 channel, which involves the adoption of a transiently populated intermediate (*up* state) leading to the thermodynamically favored *down* binding mode in the channel pore. Furthermore, they suggest that chloride anions play a relevant role in stabilizing the *down* binding mode of Amt to the wt channel, giving rise to a kinetic trapping that explains the experimentally observed pseudoirreversible inhibition of the wt channel by Amt. We propose that this trapping mechanism underlies the inhibitory activity of potent M2 channel blockers, as supported by the experimental confirmation of the irreversible binding of a pyrrolidine analogue from electrophysiological current assays. Finally, the results reveal that the thermodynamics and kinetics of Amt (un)binding is very sensitive to the V27A mutation, providing a quantitative rationale to the drastic decrease in inhibitory potency against the V27A variant. Overall, these findings pave the way to explore the inhibitory activity of Amt-related analogues in mutated M2 channel variants, providing guidelines for the design of novel inhibitors against resistant virus strains.

"Bind and Flip" mechanism
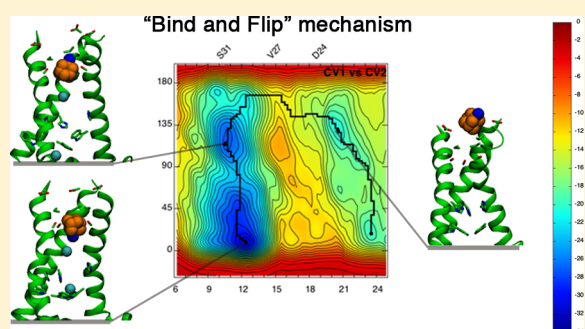
INTRODUCTION

The influenza A M2 channel is an extremely selective proton channel expressed on the viral membrane and regulated by pH changes in the interior of endosomes.[1,2] The M2 channel is a homotetrameric protein that contains an integral transmembrane four-helix channel with 97 residues per subunit, each of which comprises an intracellular C-terminal domain (residues 45–97), a transmembrane domain (residues 25–44), and an extracellular N-terminal domain (residues 1–24).[3,4] Because of its crucial role in viral life cycle,[5] it is an attractive target against influenza A virus.

The M2 channel blockers amantadine (Amt) and rimantadine (Rmt) were used for decades to treat influenza A infections since their introduction in the 1960s. However, the

Centers for Disease Control and Prevention has advised against its continued use due to the high prevalence of virus expressing drug-resistance phenotypes. This dramatically impacted the therapeutic resources available to treat flu infections, which are estimated to cause around 40 000 deaths every year in the US, and nowadays only neuraminidase inhibitors (NAI) are considered effective treatments for influenza infections.[6] However, some seasonal influenza A strains are known to be oseltamivir-resistant (although sensitive to other NAI), and with new influenza strains isolated every year, the emergence of multi-NAI-resistant strains is a serious health challenge. For this

reason, there is urgency in finding new non-NAI antiviral compounds. Most of this research has been focused on the development of novel M2-channel inhibitors that are able to overcome Amt-resistant mutations (for a recent review, see ref 7).

Three mutated variants of the M2 channel pore-lining residues have been identified in clinically relevant transmissible viruses: S31N, V27A, and L26F.[8] S31N is the most common, being present in around 95% of Amt-resistant strains. However, only mutations in position 27 have been reported to be positively selected and hence linked to drug pressure.[9] Therefore, while Amt leads to 91.0% inhibition of the proton conductance through the wild-type (wt) M2 channel at 100 μM concentration (IC$_{50}$ of 16.0 μM), the inhibition of the V27A channel is only 10.8%, thus revealing a much weaker inhibitory potency. Promising progresses in developing novel drugs targeting these mutated strains have been reported in the past years.[10−13] In particular, Wang et al. reported spiro analogues of Amt capable of inhibiting the L26F and V27A M2 mutants with good efficacy in electrophysiological and plaque reduction assays.[14−16] More recently, a polycyclic pyrrolidine has been reported to be the first nonadamantane inhibitor of the V27A variant.[17,18] On the other hand, an isoxazole derivative of Amt has been found to inhibit the S31N variant with a potency that compares with Amt in inhibiting the wt virus strain.[19,20]

Because of the pharmacological relevance of the M2 channel, a number of research efforts have been focused on characterizing the mechanism that underlies the inhibitory activity of Amt and Rmt, leading to X-ray[21−23] and NMR[24−28] structural studies on the wt channel and its V27A[29] and S31N[19,30−32] variants. In particular, solid-state NMR studies showed the existence of two Amt-binding sites in the M2 channel in phospholipid bilayers.[26] While a low affinity site was found on the C-terminal lipid-facing surface of the helices in a detergent environment or under high inhibitor concentration, the high-affinity site is located in the N-terminal channel lumen, surrounded by residues mutated in Amt-resistant strains. Moreover, the binding pocket at the pore has been identified in both the transmembrane channel, comprising residues 22−46, and the conductance domain, which includes residues 18−62.[26,33] Overall, these studies support a physical occlusion mechanism for Amt inhibition. On the other hand, while NMR data supports the binding of Rmt to the wt channel,[33] the (R)-enantiomer being the more effective inhibitor,[34] Rmt is unable to bind to the S31N variant.[30]

In spite of these progresses, little is known about the process by which Amt enters and exits the pore lumen, and the impact of mutations on the binding mechanism of Amt. This information is useful for the development of novel and more effective M2 blockers against the wt channel and its mutated variants. Here we present a theoretical study aimed at disclosing the binding/unbinding mechanism of Amt to/from the M2 channel. By combining unbiased molecular dynamics (MD) and multiple-walkers well-tempered metadynamics (MW-WTM) calculations, we provide solid evidence supporting that the (un)binding of Amt follows a sequential mechanism that involves two binding modes in the interior of the M2 channel, which can be interconverted via Amt flipping along the normal to the channel pore axis. We also propose that chloride anions play a direct role in stabilizing Amt binding through a kinetic trapping mechanism, which is supported by measurements of kinetic currents in electrophysiological assays

recorded in the presence of a pyrrolidine analogue of Amt, with equipotent inhibitory activity. Finally, the results also allow us to rationalize the impact of the V27A mutation on the relative stability of the two binding modes, providing a basis to explain the drastic reduction in inhibitory potency of Amt in the V27A channel. The results pave the way to understand the molecular determinants required for novel drugs targeting the M2 channel of influenza A virus.

■ METHODS

Setup of the Systems. The binding mode of Amt to the wild type M2 channel and its V27A variant embedded on a model bilayer of 1-palmitoyl-2-oleoyl-sn-glycero-3-phosphocholine (POPC) was studied by MD simulations and MW-WTM calculations. The M2 channel was modeled using the solid-state NMR structure (ssNMR) obtained by Sharma et al. (PDB entry 2L0J),[27] which comprises residues 22−62, and was oriented using as template the ssNMR structure with PDB entry 2KQT[26] as deposited in the Orientations of Proteins in Membranes database.[35] The X-ray crystallographic structure 3LBW[21] was used to model the position of water molecules inside the channel.

The CHARMM-GUI[36,37] web server was used to build up the initial systems. Briefly, the complex formed by the protein, the inner lumen water molecules, and the ligand was embedded on a 100 × 100 Å^2 bilayer of 1-palmitoyl-2-oleoyl-sn-glycero-3-phosphocholine (POPC) lipids. A 25 Å layer of TIP3P[38] water molecules was set up at both sides of the bilayer, and K$^+$ cations and Cl$^-$ anions were added to achieve an ionic strength of 150 mM. The Parm99SB force field[39] was used for the protein, the ligand was parametrized using the Gaff force field[40] in conjunction with RESP[41] (HF/6-31G(d)) charges as implemented in the Antechamber module of AMBER12 software package,[42] the POPC molecules were parametrized according to the GAFFlipid11 force field,[43] and Joung and Cheatham parameters[44] were used to model the counterions.

According to previous titration studies carried out with distinct constructs and environments,[45−49] the His37 tetrad was simulated considering a +2 state. Choice of the protonation state is a relevant issue that deserves a more detailed discussion. Previous NMR studies examined the pK$_a$ of His37 in constructs formed by residues 22−46 and 21−97.[46,49] The former one is shorter than the model used in our simulations, including only the transmembrane (TM) helix, while the latter one is larger, comprising the TM helix, but also the full cytoplasmic domain. The pK$_a$s for the second and third protonation in these constructs are consistent, as noted in pairs of values of 4.9 and 5.4, and 6.8 and 7.1, respectively (Table 1). On the other hand, they

Table 1. Estimated pK$_a$ Values Determined for Different Constructs of the M2 Channel

construct	His37 pK$_a$s	ref.
(22−46)	8.2, 8.2, 6.3, <5.0	45
(22−46)	7.6, 6.8, 4.9, 4.2	46
(21−97)	7.1, 7.1, 5.4	49
(18−60)	7.6, 7.6, 4.5, 4.5	47
full length	6.3, 6.3, 5.5	48

are lower than the estimated values reported for the shorter construct in the earliest measurement of the His37 pK$_a$s.[45] Furthermore, recent studies[50] performed for the construct 18−60, which contains the TM stretch, but also the amphipathic helix that interacts with the interfacial region of the lipid bilayer, estimated pK$_a$ values of 7.6 and 4.5 for the second and third protonations. Table 1 also includes the pK$_a$s reported by Miao et al. for the full length protein,[48] with estimated pK$_a$s of 6.3 and 5.5 for the second and third protonations. Even though the first two pK$_a$s are lower than the values estimated for shorter constructs, the authors indicate that at pH 6.2, where the channel should become activated, the M2 channel should be primarily in the +2 state. Moreover, the authors point out that there is little opportunity for a singly charged His37 tetrad.

Overall, in spite of the differences with the pK_as reported in previous works, which may reflect the usage of different constructs, lipid environments, and conformational heterogeneity of the tetrameric helical bundle,[48−50] the first two pK_as appear to be above the endosomal pH that activates the M2 channel, suggesting that the physiologically active state for the early activation of the M2 channel corresponds to the protonation state of +2 for the His tetrad. With regard to the ligand, Amt was simulated in the protonated form, as expected from the standard pK_a of the amine group and the acidic pH at the endosome.

Each system (apo forms of WT M2 channel and V27A mutant, and the Amt-bound complexes in *down* and *up* states; see below) comprised around 97 000 atoms, including the protein ligand complex, 265 POPC molecules, around 58 000 waters and 108 (51 K⁺; 57 Cl⁻) counterions in a simulation box of 950 000 Å³.

For each system, the geometry was minimized in five cycles that combined 3500 steps of steepest descent algorithm followed by 4500 of conjugate gradient. Thermalization of the system was performed in 5 steps of 1 ns, where the temperature was gradually increased from 50 to 298 K, while the protein, ligand, and POPC molecules were restrained with a force constant of 1 kcal mol⁻¹ Å⁻². At this point, the final structure was then used as starting model for each system (i.e., each set of 50 simulations; see below), but velocities were randomly reassigned (at 298 K) to the atoms in each independent trajectory. Then, each trajectory was subjected to a smooth equilibration simulation (20 ns), while the restraints were gradually reduced first for the POPC molecules (restraints reduced by 0.1 kcal mol⁻¹ Å⁻² at each step) and then for the protein (restraints reduced by 0.2 kcal mol⁻¹ Å⁻² at each step).

Unbiased Molecular Dynamics Simulations. Two different orientations of the ligand were explored in unbiased MD simulations. In the *down* binding mode Amt was oriented with the polar amine pointing toward the His37 plane, which was believed to be the most likely orientation according to X-ray (PDB entry 3C9J)[22] and ssNMR (PDB entry 2KQT)[26] studies. The alternative (*up*) orientation was generated through a 180 deg-rotation along the normal to the pore axis, so that the hydrophobic cage is pointing toward the His37 plane. Let us note that this orientation was proposed in previous ssNMR studies (PDB entry 2KAD)[25] and found in MD simulations of the M2 channel with distinct inhibitors.[18,51] Fifty different simulation systems were generated for each ligand−protein complex in two binding modes: *up* and *down* (accounting for a total of 200 different simulation systems). We took advantage of the NAMD 2.9 software package[52] for the production runs, which consisted of 50 ns independent trajectories per simulated system (accounting for a global simulation time of 15 μs) using SHAKE[53] for bonds involving hydrogen atoms, a time step of 2 fs, periodic boundary conditions using anisotropic constant pressure and temperature (298 K; Langevin thermostat with a collision frequency of 3 ps⁻¹), particle mesh Ewald[54] for long-range electrostatic interactions, and a cutoff of 10 Å for nonbonded interactions, and a scaling factor for 1−4 electrostatic interactions of 0.833.

Poisson−Boltzmann calculations were performed to determine the electrostatic potential in the interior of the M2 channel using the APBS program.[55] Calculations were performed for the set of 50 snapshots obtained at the end of the MD simulations (excluding cases where a transition between states, i.e., from the *up* binding mode to the *down* one, was found or upon ligand egression from the pore; see below). The snapshots were superposed through alignment of the backbone atoms of the tetrameric helix. Atomic partial charges and radii were taken from the default parameters in the Amber force field. A permittivity of 2 was assigned to the interior of the channel, whereas a value of 78.5 was used for the bulk environment. A focusing strategy was used for APBS calculations, with a finer grid of 0.25 Å/point.

Exploratory Metadynamics Simulations. Conventional metadynamics was first used to sample the physically relevant regions of the ligand binding space (for details, see page S3 in Supporting Information).[56−58] The deposition rate of the Gaussian bias terms was set to 1 ps and Gaussian height was set to 0.1 kcal mol⁻¹. The initial position was set to equilibrated systems reproducing the crystallographic binding mode.

To obtain an overall free energy profile of the ligand binding to the M2 channel, we used three different collective variables, termed here CV1, CV2 and CV3 (see Figure S1 in Supporting Information). Specifically, CV1 consisted of the distance between the center-of-mass (COM) of the Cα atoms of the four H37 residues and the COM of the heavy atoms of the ligand. CV2 accounted for the tilt angle of the ligand. It was characterized as the angle defined by the COM of Cα of the four H37 residues, the COM of the heavy atoms of the hydrophobic cage of the ligand, and the position of the nitrogen atom of the ligand amine. Finally, CV3 accounted for the distance of the closest chloride anion to the S31 tetrad in the channel. To this end, we selected and monitored two chloride atoms that were allowed to enter and exit the pore of the channel (see below). The minimum distance CV defined in PLUMED plugin[59,60] was used to monitor the lowest distance between those two anions and the COM of the oxygen atoms of the four S31 side chain residues. A β value of 500 was used to ensure differentiability of the variable (i.e., β controls the smoothness of the mapping from the high-dimensional space to the low-dimensional space). Proper restraining walls were used to maintain other anions away from the protein and to keep the selected ones between a range of 1 and 25 Å. For all the CVs, the Gaussian width was set to 0.2 units of the CV (CV1 = Å, CV2 = radians, CV3 = Å).

Multiple-Walkers Well-Tempered Metadynamics. Further refinement of the energetic landscape was obtained applying well-tempered metadynamics[61] combined with the multiple-walkers technique (MW-WTM).[62] To this end, several simulations were run to explore the same free energy surface and interact by contributing to the same history-dependent bias potential. The deposition rate of the Gaussian bias terms was set to 1 ps, their initial height to 0.5 kcal mol⁻¹ and a bias factor of 20 ($T + \Delta T = 5960$ K). Initial positions for each walker were set at different regions of the CV space found during the metadynamics simulation. The system was simulated for a total of 0.5 μs using 6 walkers, and the bias potential was updated every 0.2 ps.

Electrophysiology Assays. A/M2 cDNA from influenza A/Udorn/307/72 H3N2 virus strain was cloned into pSUPER vector for the expression in *Xenopus laevis* oocytes. A/M2 V27A mutant was generated by QuikChange site-directed mutagenesis kit (Agilent Technologies). The synthesis of cRNA and microinjection of oocytes have been described previously.[63] Oocytes were perfused at room temperature in Barth's solution (in mM: 88 NaCl, 1 KCl, 2.4 NaHCO₃, 0.3 NaNO₃, 0.71 CaCl₂, 0.82 MgCl₂, and 15 HEPES for pH 8.5 or 15 MES for pH 5.5). Amt and compound 4 were dissolved in DMSO and applied (100 μM) at pH 5.5 when the inward current reaches maximum. Currents were fitted to a single exponential function ($y = e^{-t/\tau}$ + constant with $r > 0.94$) and the time constant τ was used to calculate the forward rate constant (k_{on}) after addition of Amt and compound 4 ($k_{on} = 1/[\text{compound}] \ \tau$). Currents were analyzed with pCLAMP 8 software package (Axon Instruments, Sunnyvale, CA).

■ RESULTS AND DISCUSSION

The available experimental data support that Amt binds the pore of the M2 channel (see above), it being widely assumed that the protonated amine points toward the His37 plane. However, it is unclear whether this may be the unique binding mode of Amt in the channel lumen. Furthermore, the assumption that Amt adopts the same binding mode in other mutated variants of the M2 channel remains to be elucidated. Here we present the results of a theoretical study that aims to provide answers to the preceding questions, which would be valuable for understanding the inhibitory potency of Amt-related analogues in wt and mutated M2 channels and guide the design of novel M2 channel inhibitors.

Simulations of Amt Bound to the Wild-Type M2 Channel. Both crystallographic and NMR data have consistently shown that Amt is accommodated in the pore of the wt M2 channel just below the Val27 valve, with its center-of-mass (COM) aligned with the plane defined by Ser31

residues. Furthermore, Amt is most likely oriented with its amino group pointing toward the His37 tetrad. The structural stability of this binding mode, which will be denoted *down* hereafter (Figure 1), was supported by previous MD simulations.[15,18,64]
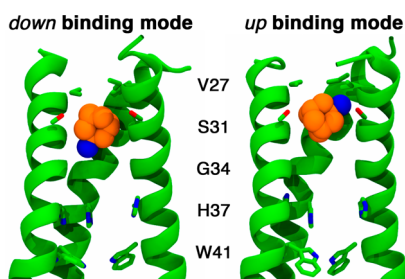

Figure 1. Representation of Amt (shown as orange spheres) bound to the wt M2 channel in the *down* and *up* binding modes. The side chains of residues His37 and Trp41 are shown as green sticks. For the sake of clarity, only three helices of the tetrameric channel are shown.

In order to obtain an exhaustive sampling of the *down* binding mode, we have run 50 independent MD simulations of Amt in the channel pore, covering a total simulation time of 2.5 μs. Simulations yielded stable trajectories in all cases, where the overall structure of the tetrameric bundle was well preserved. Furthermore, the occurrence of large structural alterations in the TM segment was also checked, but the analysis of the trajectories confirmed the structural integrity of the helices. In particular, the presence of relevant kinks was verified using KinkFinder,[65] and the results confirmed that the helices in the bundle do not present significant kinks (typically lower than the threshold value of 20 degrees; see page S9 and Figures S2–S4 in the Supporting Information for details). Moreover, the results consistently showed that Amt was firmly bound at the pore with a precise geometrical arrangement in the channel lumen. On average, the *down* binding mode was characterized by a distance from the amine nitrogen of Amt to the plane defined by the tetrad of His37 Cα atoms ($d_{\text{N-His37}}$) close to 7.8 Å, whereas the COM of the ligand was located close to the plane of Ser31 Cα atoms (distance less than 0.4 Å; see Figure 1). Moreover, the principal axis of Amt was slightly deviated from the pore axis, as noted by a tilt angle (defined as the angle

between the amine N, the COM of Amt, and the COM of the His37 Cα atoms) close to 16 degrees.

Adoption of the *down* binding mode implies that Amt must compensate the large electrostatic destabilization arising from the spatial proximity between the protonated amine group and the positive charges in the His37 plane. Thus, Poisson–Boltzmann calculations[55] pointed out that the electrostatic repulsion is estimated to be close to 80 kcal/mol. How is this repulsive interaction counterbalanced? Our simulations indicate that the presence of anions in the channel is crucial for compensating the electrostatic destabilization. Thus, the isocontour density maps of chloride anions reveal the presence of two favorable areas in the interior of the channel, typically located above the Trp41 tetrad and above the His37 tetrad (Figure 2). In fact, even the analysis of MD simulations (50 ns) run for the apo form of the wt channel shows the presence of Cl$^-$ anions in the pore, although in this case they are primarily located between the planes of His37 and Trp41 (Figure 2).

The presence of chloride anions in the interior of the channel may be striking for a proton transport channel. However, it is worth noting that the analysis of the whole set of trajectories run for both apo and Amt-bound forms of the M2 channel revealed the absence of Cl$^-$ passage through the channel (for details, see page S12 and Figure S5 in the Supporting Information). On the other hand, the finding that chloride anions may occupy the area proximal to the Trp41 tetrad has been described in previous studies.[66–68] To the best of our knowledge, this was first reported by Mustafa et al.[66] in short (10 ns) MD simulations of the 22–46 construct, as they noticed the presence of Cl$^-$ anions at the level of the Trp41 tetrad for the +2 and +3 states, and even that they were able to enter the His37 selectivity filter in this latter state. Likewise, the results reported by Wei and Pohorille[67] indicated that chloride anions penetrate the pore in all charged states of the wt M2 channel, but not for the fully unprotonated form. Furthermore, they also found that the position of the Cl$^-$ anions depends on the charge state, and for the diprotonated form of the channel they occupied the space between His37 and Trp41 planes. It is worth noting that these findings were obtained using a different force field (CHARMM22) and simulation conditions. Similar results were found by Gkeka et al., who reported the presence of 2–3 Cl$^-$ anions inside the pore, close to the protonated His37 residues.[68] Furthermore, it is also worth noting that phosphate anions may also bind to the positively charged His37
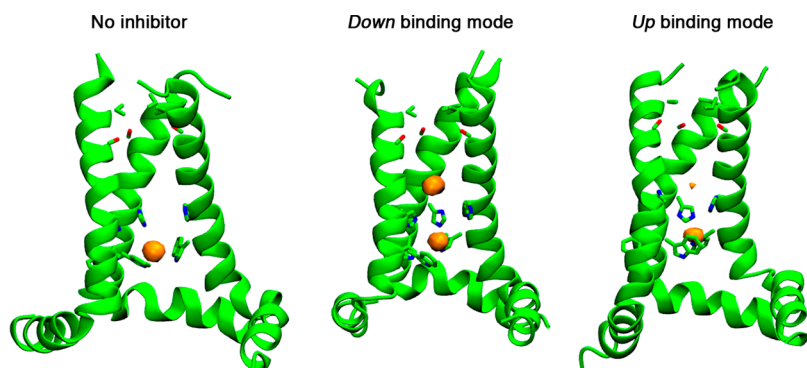

Figure 2. Isodensity maps of chloride anions in the interior of the pore for the wt M2 channel in (left) the apo form, and in the presence of Amt, which was oriented in the (middle) *down* and (right) *up* arrangements in the interior of the channel. The orange isocontour corresponds to an isodensity value of 0.15 g/cm³. His37 and Trp41 residues are shown as sticks. For the sake of clarity, only three helices of the tetrameric channel are shown.

sites.[67] Remarkably, the presence of a chloride anion between residues Gly34 and His37 on the 4-fold axis of the channel has been recently reported for the X-ray structure of the S31N mutated channel.[69]

The presence of chloride anions in the pore has a strong influence on the nature of the electrostatic potential in the interior of the channel, which is highly positive in the absence of anions, but slightly positive when Cl⁻ anions are present near the His37 sites (Figure 3). Overall, it can be argued that the
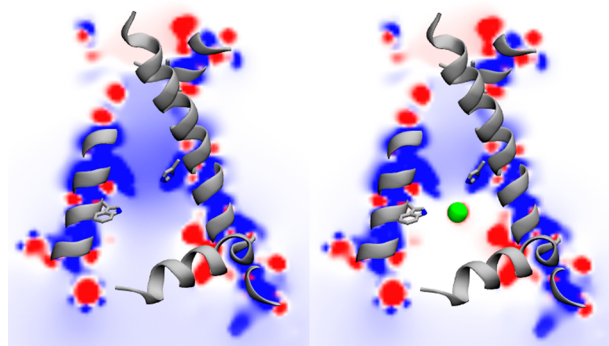
Figure 3. Representation of the electrostatic potential (kcal/mol) in a plane passing through the interior of the M2 channel in (left) absence and (right) presence of chloride anions. Isocontours range from +12 (blue) to −12 kcal/mol (red). His37 and Trp41 residues are shown as sticks.

penetration of chloride anions in the pore is a key event for assisting the binding of Amt by screening the electrostatic repulsion of the protonated amine with the His37 residues.

Can Amt Adopt an Alternative Binding Mode? Besides the *down* binding mode, it has been suggested that Amt may adopt an alternative arrangement, in which the protonated amine is pointing toward the N-terminus of the channel. This roughly corresponds to a 180-degree inversion of Amt along an axis perpendicular to the channel pore, leading to the *up* binding mode (Figure 1). In fact, Leonov et al.[70] reported that Amt was substantially restrained to the *up* orientation in the region located between Val27 and Gly34. Similar trends were reported for Rmt, which was found in the *up* orientation when it was above the His37 tetrad.[71]

With the aim to compare the features of this binding mode with the *down* arrangement, 50 independent 50 ns MD simulations were run starting from the *up* binding mode. The trajectories were generally very stable in this time scale (see also page S9 and Figure S2 in the Supporting Information), suggesting that Amt adopts a well-defined orientation, which is characterized by a distance from the amine nitrogen to the His37 Cα plane ($d_{\text{N-His37}}$) close to 14.0 Å, whereas the COM of the ligand is close to the plane of Ser31 Cα atoms. Moreover, the principal axis of Amt slightly deviates from the pore axis, as noted by a tilt angle close to 135 degrees. The analysis of the trajectories also reveals the presence of chloride anions in the interior of the pore. However, in contrast to the *down* binding mode, where two almost identical peaks were found in the pore, the isodensity map obtained for the *up* binding mode shows a major peak located close to the Trp41 tetrad, thus resembling the distribution density obtained for the apo M2 channel (see Figure 2).

In spite of the remarkable stability of the *up* binding mode, it is worth noting that in three simulations Amt was able to flip

inside the pore and eventually adopt the *down* binding mode, which was then retained until the end of the simulations. This suggests that the *down* binding mode may be thermodynamically more stable than the *up* orientation, although there must be a non-negligible barrier for flipping of the ligand inside the channel, which slows down the *up* → *down* transition. Finally, none of the trajectories showed the release of Amt to the channel mouth, which supports the existence of a significant kinetic barrier that prevents release of Amt from the pore.

Binding Mechanism of Amt to Wild Type M2 Channel. The limited sampling achieved from unbiased MD simulations makes it necessary to be cautious about the functional role of *down* and *up* binding modes, giving rise to a number of questions related to the relative stability of these states and the origin of the barriers for ligand (un)binding. With the aim to explore the (un)binding mechanism to the M2 proton channel, we first carried out conventional metadynamics starting from the *down* binding mode. To this end, preliminary computations were performed considering two collective variables (see Figure S1 in the Supporting Information), which were defined as the distance between the COM of Amt to the central point of the His37 Cα tetrad (CV1), and the tilting of the inhibitor (CV2). However, these simulations yielded inconsistent results due to the perturbation arising from the exchange of chloride anions between the channel and the bulk solvent during the simulation. These exchanges occurred as uncontrolled stochastic events, calling for an explicit treatment through a dedicated collective variable. As revealed by unbiased MD simulations, up to two chloride ions can be accommodated inside the channel, depending on the binding state and Amt orientation (see Figure 2). Therefore, we decided to map the position of two of such anions confined within the pore by calculating their minimum distance from the S31 tetrad (CV3; Figure S1 in the Supporting Information). This choice permits one to monitor the position of the closest anion to the inhibitor's binding site, which is supposedly the most relevant for Amt (un)binding, but it also accounts for natural exchanges between chloride anions. Moreover, mapping the position of two anions through a single collective variable was also instrumental to moderate the computational cost of metadynamics simulations, which is known to scale approximately exponentially with the number of CVs.

The analysis of the free energy surface (FES) determined from conventional metadynamics (Figure S6 in Supporting Information) allowed us to identify three relevant minima on the collective variable space (Figure S6B and S6C). The first basin (I) corresponds to the *down* binding mode, which is characterized by a distance to the His37 tetrad of 10 Å and a tilt angle of 10 degrees. Furthermore, a chloride anion is found above the His37 plane, and another is located above the Trp41 plane. The second basin (II) corresponds to the *up* binding mode, as noted in values of 11 Å and 135 degrees for the two first collective variables. Finally, the last basin (III) denotes a wide and diffuse area spanning distances to the His37 tetrad of 18−21 Å and tilt angle of 90−170 degrees. These results supported the existence of the *up* binding mode as an energetically intermediate state in the binding pathway leading to the *down* arrangement, and allowed us to hypothesize that the binding of Amt would require the flip of compound in the channel pore upon conversion between *up* and *down* states.

With the aim to obtain a chemically more accurate representation of the FES, MW-WTM calculations were run. The key features of the FES obtained from conventional
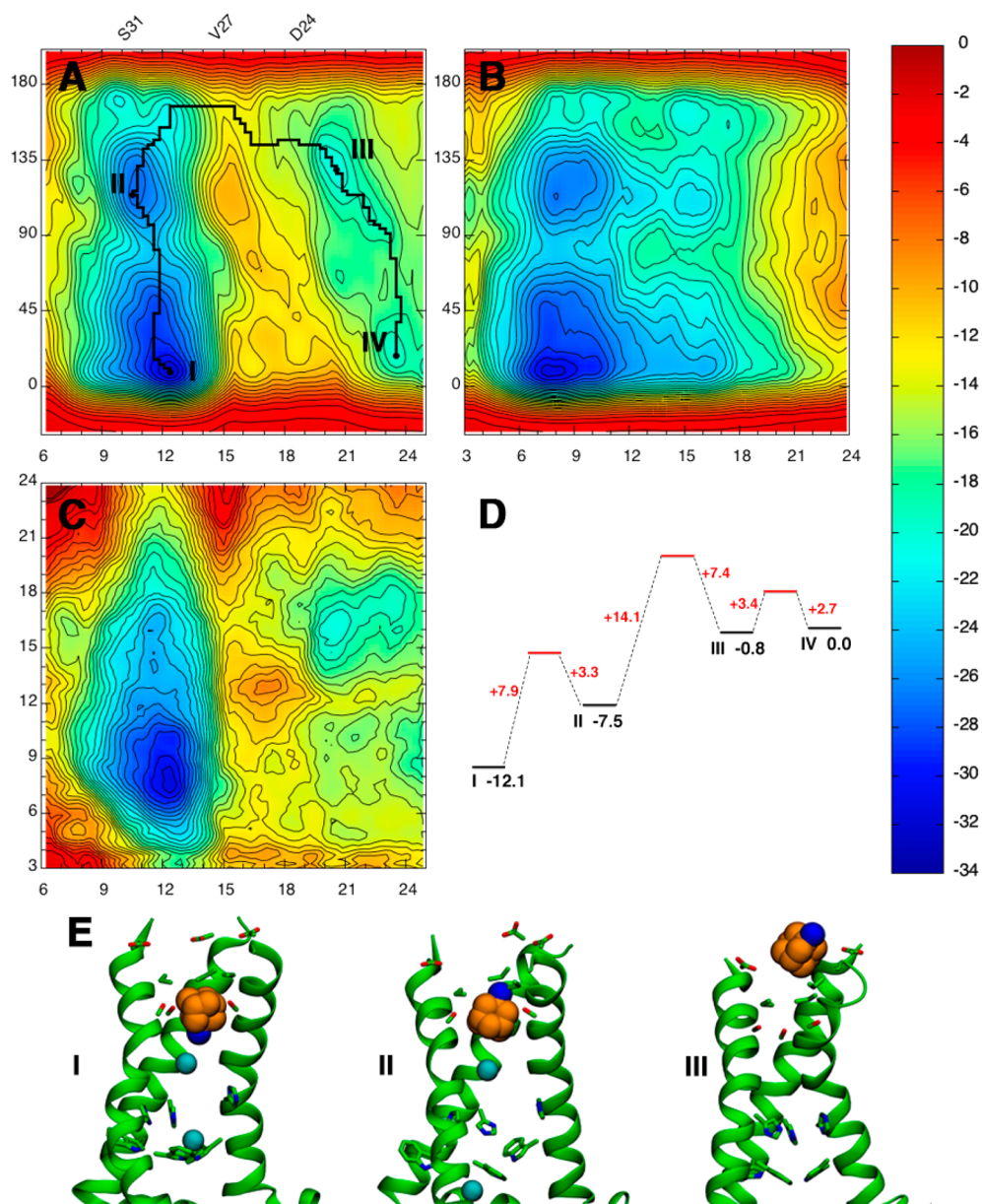
Figure 4. Free energy surface maps (values in kcal/mol) in the collective variable space obtained with the MW-WTM calculations for the binding of Amt to the wt M2 channel. (A: CV2 (degrees; y-axis) versus CV1 (Å; x-axis); B: CV2 (degrees; y-axis) versus CV3 (Å; x-axis); C: CV3 (Å; y-axis) versus CV1 (Å; x-axis); the location of selected residues along the CV1 variable is indicated in panel A). The interval of the free energy isocontours is 1 kcal/mol. (D) Schematic representation of the relative stabilitiy of the different basins. Horizontal black lines denote the different states found in the free energy surface, and are accompanied by the relative free energy (in black; kcal/mol). Horizontal red lines denote the saddle points between minima, and are accompanied by the free energy change relative to the proximal minima (in red; kcal/mol). (E) Representative structures of the basins obtained from MW-WTM calculations for Amt in the pore of the wt M2 channel. Carbon/nitrogen atoms of Amt are shown as orange/blue-colored spheres, carbon/nitrogen atoms of His37 and Trp41 residues are displayed as green/blue sticks, and chloride anions as cyan spheres.

metadynamics were retained in the MW-WTM FES, preserving the relevant minima on the collective variable space (Figure 4). However, subtle differences can be found. Thus, in contrast to the results obtained from conventional metadynamics (see Figures S6B and S6C), the well depth of the *up* binding mode is more negative, it being still less favored than the *down* state, but more stable than the basin with Amt at the entrance of the channel. Furthermore, this latter state contains two nearly degenerate minima (III and IV in Figure 4), in which the protonated amine of Amt forms a salt bridge with the carboxylate group of Asp24. In one case, the hydrophobic cage is pointing toward the pore (tilt angle of 130 degrees), and

in the other (IV) the adamantane cage is pointing toward the bulk solvent (tilt angle close to 20 degrees). This suggests the lack of severe steric constraints at the entrance of the channel, allowing Amt to adopt multiple arrangements in the channel mouth. At this point, let us note that the rate of inhibition of truncated mutants of the M2 channel by Amt differs by a factor of ~2 compared to the full-length wt channel, thus giving support to the previous suggestion.[72]

The FES shows that the *down* binding mode (I) is the most stable minima, it being favored by 4.6 kcal/mol with regard to the *up* binding mode (basin II). This free energy change compares with the difference (~7 kcal/mol) reported from

umbrella sampling calculations, even though these studies were performed for the channel with neutral His37 residues.[73] The $down \rightarrow up$ transition is associated with a barrier of 7.9 kcal/mol, whereas the barrier for the $up \rightarrow down$ transition is estimated to be 3.3 kcal/mol. From basin II egression of Amt is preceded by the transition to the mouth of the channel (III), a process destabilized by 6.7 kcal/mol. The barrier for the transition from the up binding mode to the entry of the channel is 14.1 kcal/mol, while the barrier for the reverse transition is only 7.4 kcal/mol. The location of this barrier coincides with plane formed by the V27 tetrad (Figure 4A), and hence can be attributed to the steric hindrance required for the passage of Amt to the N-terminus. In the channel mouth, the two quasidegenerate minima (III and IV) differ by 0.8 kcal/mol and can be interconverted through a small barrier close to 3 kcal/mol.

Overall, release of Amt from the $down$ state to the mouth of the channel is associated with a net barrier of 18.7 kcal/mol, and is thermodynamically disfavored by 12.1 kcal/mol. This latter value is lower than the destabilization reported in previous studies (23.5 kcal/mol),[73] although it is worth noting that present calculations do not include the contribution due to Amt liberation to the bulk solvent (see below). On the other hand, it is worth noting that the pathway leading to the direct egression from the $down$ state to the entry of the channel (I $\rightarrow$ IV) must overcome a larger barrier (estimated to be slightly larger than 20 kcal/mol). Thus, MW-WTM calculations (as well as conventional metadynamics simulations; see Figure S6 in the Supporting Information) support the release of Amt via the transient up state. This mechanism may also operate for compounds with a size similar to Amt. However, one may deduce that this mechanism may not be valid for inhibitors with size-enlarged hydrophobic cages, as the flipping inside the channel may presumably lead to steric clashes, and hence to a larger barrier.

What is the effect of the chloride anion proximal to the ligand on the energetics of Amt (un)binding? A finer inspection of the FES maps in Figure 4 reveals that the $down \rightarrow up$ transition is largely affected by the stabilizing electrostatic interactions with the proximal anion in the channel lumen. Thus, the $down$ state is penalized by 6.6 kcal/mol upon release of the Cl^- anion, while a lower, but still significant destabilization of 4.4 kcal/mol is found for the up state. Accordingly, the stability of the $down$ and up states changes from −12.1 to −5.5 kcal/mol ($down$), and from −7.5 to −3.1 kcal/mol (up). Overall, release of the chloride anion from the channel pore makes the $down$ state to be favored only by 2.4 kcal/mol relative to the up binding mode, whereas the relative stability of the $down$ state with regard to basin IV would be reduced from −12.1 kcal/mol to only −5.7 kcal/mol, which would imply a drastic reduction in the inhibitory potency. These findings agree with the results from a previous study[74] about the effect of a chloride anion on the Amt orientation in the pore, as Amt flipped between facing the C- and N-terminus in the absence of Cl^-, but no flipping was found upon presence of Cl^-. Therefore, (un)binding of Amt should be regarded as a dynamic process, where the FES may be shaped not only by the structural fluctuations sampled by the tetrameric assembly,[75,76] but also by the trapping of chloride anions into the channel pore from the C-terminal entry.

Simulations of Amt Bound to the V27A Channel. Mutation of Val27 to Ala causes a drastic reduction in the inhibitory activity of Amt. This suggests that the $down$ binding mode should be largely destabilized in the V27A channel, but it is unclear whether Amt can bind the mutated channel in a distinct orientation and how the V27A mutation may affect the mechanism of ligand binding/unbinding and the overall energetics of the entry/release of Amt.

To answer these questions, the behavior of Amt bound to the V27A channel was explored by means of unbiased MD simulations, which also showed the structural integrity of the simulated systems (see page S9 and Figure S2 in the Supporting Information). Among the 50 simulations started from the $down$ binding mode, they ended up with Amt in the up orientation in 44 trajectories, and in 6 cases Amt even escaped from the pore to the mouth of the channel. On the other hand, when simulations started from the up binding mode, Amt remained stable in 45 cases and was released from the pore in the rest of simulations. Overall, these findings demonstrate that the $down$ binding mode is largely destabilized by the V27A mutation, and that Amt should bind the mutated channel only in the up arrangement. In this binding mode, the COM of the ligand was located at ~12.3 Å from the His37 Cα plane, and the tilt angle was close to 157 degrees. Compared to the same binding mode to the wt channel, the V27A mutation causes the ligand to be displaced by ~1 Å toward the N-terminus, and aligned closer to the channel axis.

The preference of the up arrangement can be realized from the electrostatic repulsion between the protonated amine of Amt and the diprotonated His37 tetrad, and by the lack of a significant population of chloride anions in the interior of the pore. Although the analysis of unbiased MD simulations shows the presence of Cl^- anions in the channel, a single peak is observed in the isodensity distribution between the planes defined by His37 and Trp41 tetrads (Figure 5). Furthermore,
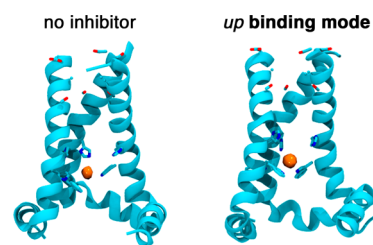

Figure 5. Isodensity maps of chloride anions in the interior of the pore for the V27A channel in (left) the apo form, and in the presence of Amt, which was oriented in the (right) up arrangement in the interior of the channel. The orange isocontour corresponds to an isodensity value of 0.15 g/cm^3. Carbon/nitrogen atoms of His37 and Trp41 residues are shown as cyan/blue sticks. For the sake of clarity, only three helices of the tetrameric channel are shown.

there is large resemblance between the distribution obtained for both apo and Amt-bound states in the V27A channel, which suggests a negligible electrostatic effect of the Amt protonated amine on the distribution of chlorine anions, in contrast to the double peak found for the $down$ binding mode of Amt in the wt M2 channel (see Figure 2).

In order to quantify the energetics of Amt (un)binding to the V27A variant, the FES was determined by using exploratory conventional metadynamics simulations with the same set of collective variables utilized for the wt channel (see Figure S7 in the Supporting Information), and later refined through MW-WTM calculations (Figure 6). Compared to the wt M2 channel, the results pointed out a drastic alteration in the FES, since the $down$ binding mode (I) was largely destabilized in the
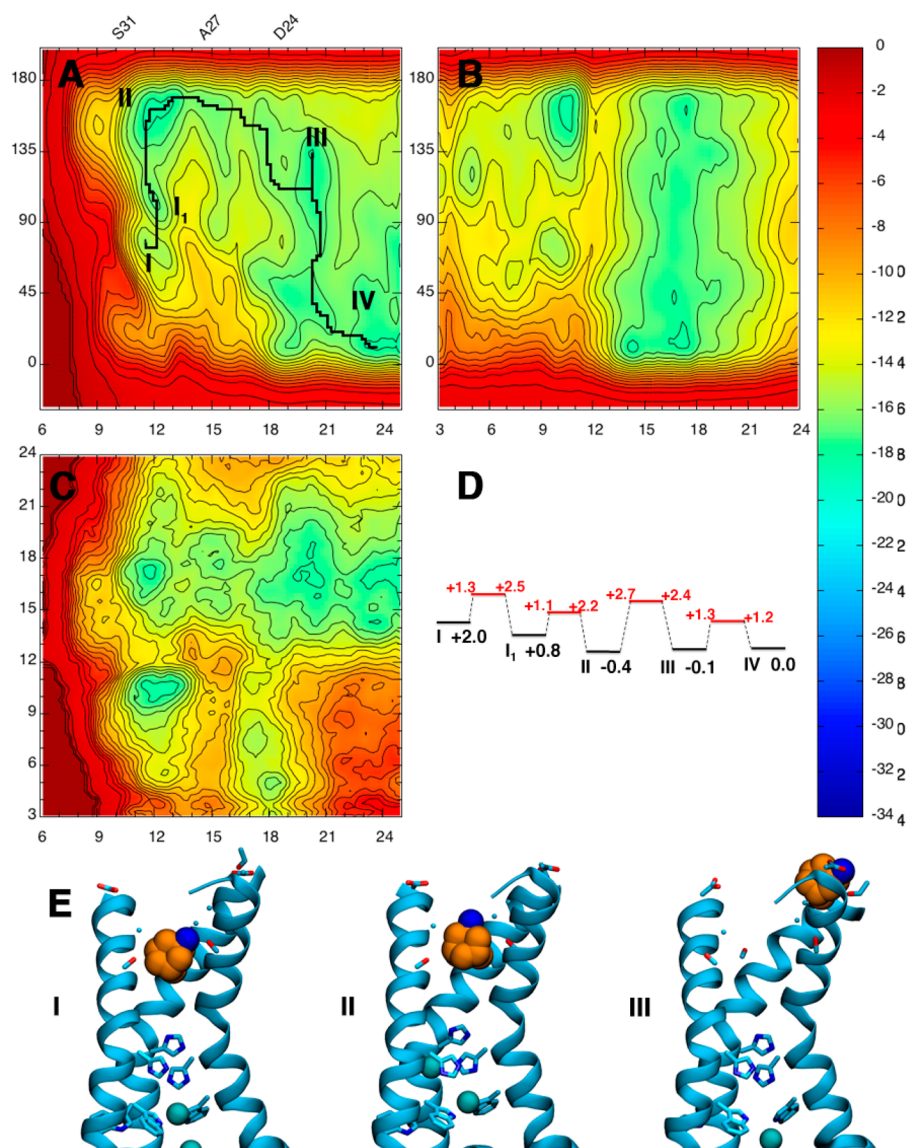
Figure 6. Free energy surface maps (values in kcal/mol) in the collective variable space obtained with the MW-WTM calculations for the binding of Amt to the V27A M2 channel. (A: CV2 (degrees; *y*-axis) versus CV1 (Å; *x*-axis); B: CV2 (degrees; *y*-axis) versus CV3 (Å; *x*-axis); C: CV3 (Å; *y*-axis) versus CV1 (Å; *x*-axis); the location of selected residues along the CV1 variable is indicated in panel A). The interval of the energy isocontours is 1 kcal/mol. (D) Schematic representation of the relative stabilitiy of the different basins. Horizontal black lines denote the different states found in the free energy surface, and are accompanied by the relative free energy (in black; kcal/mol). Horizontal red lines denote the saddle points between minima, and are accompanied by the change in free energy from the proximal minima (in red; kcal/mol). (E) Representative structures of the basins obtained from MW-WTM calculations for Amt in the pore of the V27A M2 channel. Carbon/nitrogen atoms of Amt are shown as orange/blue-colored spheres, carbon/nitrogen atoms of His37 and Trp41 residues are displayed as cyan/blue sticks, and chloride anions as cyan spheres.

mutated variant, whereas the *up* binding mode is slightly more stable compared with Amt bound at the N-terminus of the channel. Thus, the *down* state is destabilized by 2.4 kcal/mol with regard to the *up* binding mode (II), and the *down* → *up* transition occurs through an intermediate state (I$_1$) with barriers less than 1.4 kcal/mol. This suggests that the *down* state has a negligible contribution to the binding of Amt to the V27A variant, in agreement with the results obtained from unbiased MD simulations (see above). The *up* state in the mutated channel retains the features described above for the same binding mode in the wt channel, as noted in a distance from the Amt COM to the His37 tetrad close to 12 Å and a tilt angle spanning from 115 to 150 degrees. On the other hand, the well depth of the *up* minimum is stabilized by 0.4 kcal/mol relative to states III and IV, where Amt interacts with Asp24.

Furthermore, the transition from the *up* binding mode to the channel mouth is limited by a small barrier of 2.7 kcal/mol. Overall, these findings provide a simple explanation for the drastic reduction of inhibitory activity of Amt in the V27A M2 channel.

Comparison of Figures 4 and 6 also points out that transition of Amt from state III, where it interacts with Asp24 residues, to state II, which corresponds to the *up* binding mode, is more penalized in the wt channel (barrier of 7.4 kcal/mol) than in the V27A variant (barrier of 2.4 kcal/mol). This reflects the free energy cost associated with dehydration of the protonated amine (see Figure 7). Thus, the radial distribution of water molecules around the amine nitrogen for the *up* binding mode exhibits two peaks at around 2.8 and 3.6 Å, but the intensity is ~2-fold higher in the mutated channel than in the wt form.
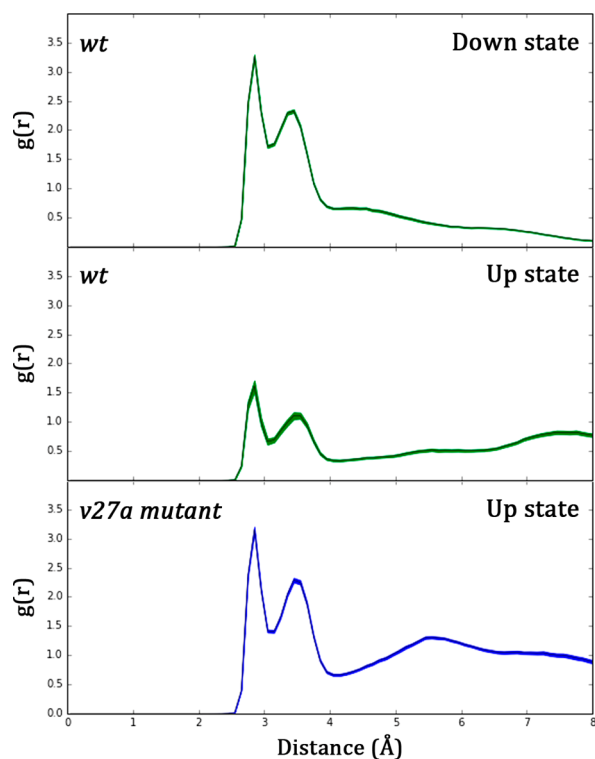
Figure 7. Radial distribution of water molecules around the protonated amine nitrogen of Amt in the *down* and *up* binding modes to the wt M2 channel, and the *up* binding mode to the V27A variant. The mean values and the standard error of the mean are shown in the plots. The analysis was performed for the snapshots sampled in the last 10 ns of the simulations.

This reflects the widening of the pore triggered by the Va27 → Ala mutation (see Figure S8 in the Supporting Information), which permits binding of Amt to the V27A channel with lower dehydration penalty relative to the wt M2 channel. On the other hand, Figure 7 also shows that the radial distribution of water molecules for the *down* state in the wt channel is similar to the profile found for the *up* state in the V27A variant. Therefore, the larger binding of Amt to the wt channel not only arises from the electrostatic stabilization afforded by chlorine ions, but also from the recovery of hydrating water molecules after transition from the *up* state the *down* binding mode.

Binding Mechanism and Functional Implications. The preceding results point out that (un)binding of Amt to the wt

channel follows a sequential mechanism characterized by two key features (Figure 8): (i) binding occurs through transition via the transiently populated *up* state, and (ii) binding is assisted by the presence of chloride anions in the pore. Thus, Amt binds to the channel mouth, where it is trapped by electrostatic interactions with Asp24. The hydrophobic cage can adopt multiple orientations, and eventually it reorients toward the channel pore in a process favored by the loss of unfavorable interactions with surrounding water molecules, while it faces the hydrophobic surface of the Val27 tetrad. From this state, thermal fluctuations of the helices facilitate crossing through the Val27 filter, and Amt fills the channel lumen in the *up* binding mode. Finally, rotation of Amt in the binding site leads to the thermodynamically most favored *down* state. Without Cl^- anions, this process is stabilized by 5.7 kcal/mol. However, the presence of chloride anions in the channel enhances the thermodynamic stability by near 6 kcal/mol, leading to an overall stabilization of 12.1 kcal/mol.

It is worth noting that the free energy difference estimated for the transition of Amt from the entrance of the channel to the *down* state (12.1 kcal/mol) is not strictly the binding affinity, as it omits the free energy contribution due to release of Amt to the bulk aqueous solvent due to the application of the distance constraint in CV1, which impeded the liberation of Amt beyond the channel mouth. This constraint was imposed to guarantee a full sampling of the ligand in the interior of the channel, while keeping this sampling under feasible computational demands. Nevertheless, it is instructive to compare this quantity with the experimental binding affinity (apparent K_i of 0.3×10^{-6} M),[77] which amounts to 9 kcal/mol. First, the apparent K_i was determined through electrophysiological current assays performed with oocytes expressing the M2 channel, and by measuring the fraction of remaining current after 2 min exposure to Amt. Since the Amt-induced blockage of the current is nearly irreversible, the assay does not properly correspond to an equilibrium measurement of the inhibitory constant. However, this value compares well with the estimated binding constants obtained for a shorter M2 channel from surface plasmon resonance (residues 22−46; K_d of 0.91×10^{-6} M),[78] and from isothermal calorimetry (residues 21−61; K_d of 2.3×10^{-6} M).[72] Second, as noted above, the calculated free energy difference reflects the transition from the *down* binding mode to the channel mouth, where Amt forms salt bridge interactions with Asp24. Accordingly, one should account for the free energy contribution of releasing Amt from the channel mouth to bulk solvent, which can at first sight to be
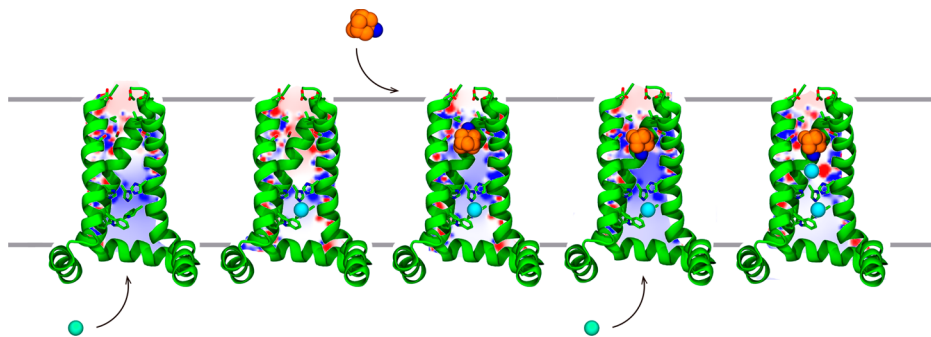

Figure 8. Representative scheme iIlustrating the stepwise mechanism for Amt binding to the wt M2 channel. Carbon/nitrogen atoms of Amt are shown as orange/blue-colored spheres. Chloride anions are shown as green spheres. For the sake of clarity, only three helices of the tetrameric channel are shown as green cartoon embedded in the lipid membrane.

approximated as the cost of breaking the salt bridge between Amt and Asp24. There is evidence that solvent-exposed salt bridges generally have a marginal stability.[79−83] For instance, Hendsch and Tidor reported that, depending on their solvent exposure, the association free energy of a salt bridge may range from −0.9 to +2.2 kcal/mol,[83] suggesting that the theoretical binding affinity may be slightly overestimated. Hence, inclusion of this term likely accounts for a significant fraction of the difference between the free energy difference estimated from these calculations and the experimental binding affinity. Third, we cannot completely rule out an uncertainty in the experimental value due to the structural differences between the M2 channel used in simulations, which relies on the ssNMR structural model 2L0J (comprising residues 22−62), and the full-length channel or shorter constructs expressed in experimental assays,[72,77,78] although the rate of inhibition of the truncated mutants by Amt was found to compare well with the range of variation seen for the M2 channel from different Amt-sensitive strains.[72,77] Finally, an additional source of uncertainty may arise from the potential partition of a fraction of Amt in the membrane, as noted in previous experimental studies.[84]
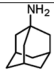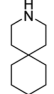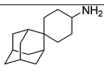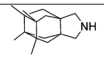
The dissociation rate constant determined for Amt from electrophysiological assays has been estimated to be 3×10^{-4} s^{-1},[72] which would correspond to a free energy barrier of 22 kcal/mol at 298 K according to Eyring's equation. The results derived from MW-WTM simulations indicate that the rate limiting step for egression of Amt is determined by the transition from the *up* binding mode to the channel mouth, with a barrier of 14.1 kcal/mol, which is near 2-fold larger than the barrier for the *down* → up transition. Taken together, release of Amt from the *down* state would imply a net destabilization of 18.7 kcal/mol, which is in remarkable agreement with the experimental value, especially keeping in mind the assumptions inherent to both experimental assays and theoretical simulations. Remarkably, these results provide a basis to justify the pseudoirreversible behavior observed for Amt in electrophisiological assays, as noted in the fact that the inhibition of the wt M2 channel caused upon addition of Amt was not reversed over a 5 min period upon removal of the drug.[85] This finding suggests that the drug was tightly bound to the interior of the channel, and this reflects the large barrier for egression of Amt from the *up* state to the entrance of the channel.

Overall, we propose that Cl$^-$ anions take an active role in assisting the Amt binding (i) by reducing the positive electrostatic potential created by the protonated His37 in the channel lumen, and (ii) by screening the electrostatic repulsion between the positive charges of protonated Amt and His37 residues though insertion of a Cl$^-$ anion in between them. In fact, for certain simulations where chloride anions were absent from the interior of the pore, Amt was rapidly released toward the channel mouth (data not shown). Of course, the classical treatment of the simulated system does not permit the release of protons from the protonated His37 residues, a process that has often been assumed to occur upon binding of Amt.[73,74,86,87] Nevertheless, under the acidic conditions at the endosome, where the pH gradient would tend to maintain the channel in a +2 state, Occam's razor make us to support the electrostatic stabilization of chloride anions, which have fast exchange to/from the interior of the channel.

What Makes a Compound to Be a Potent M2 Channel Inhibitor? On the basis of the preceding findings, the answer

to this question may be related to the ability of a compound to adopt the *down* orientation assisted by the electrostatic stabilization with chloride anions. In turn, this can be expected to depend on the size and nature of the hydrophobic cage, as these chemical features will influence the binding within the channel lumen. Among the inhibitors reported in the literature,[7,88] this can be examined by considering the spiro compounds **1−3**[14,15,89] and the pyrrolidine derivative **4**,[18] which have inhibitory potencies that are almost identical (**2−4**) or better (**1**) than Amt against the wt M2 channel (Table 2).

Table 2. Geometrical Parameters (Maximal Length, Å; van der Waals Volume: Å^3) and Inhibitory Potencies (Measured as IC$_{50}$ values, μM) of Selected Inhibitors against the wt M2 Channel and Its V27A Variant

Compound		Length	Volume [a]	IC$_{50}$ [b] (wt)	IC$_{50}$ (V27A)
Amt	NH$_2$	4.0	166	16.1	>500
1	H N	5.9	182	0.9	>200
2	NH$_2$	6.9	198	12.6	84.9
3	NH$_2$	7.8	244	18.7	0.3
4	NH	5.6	254	18.0	0.7

[a]Determined with MOE (Molecular Operating Environment).[93] [b]Data from refs 14, 15, 18, and 89.

Compared to Amt, these compounds afford a maximal longitudinal and volume expansion of 95% (**3**) and 53% (**4**), respectively. However, these drastic changes in size and shape have only a minor effect on the inhibitory potency (see Table 2). On the other hand, the most potent compound (**1**; IC$_{50}$ of 0.9 μM) has a maximal length corresponding to ∼50% increase relative to Amt, which may be considered to be the optimal length to fill the longitudinal axis of the channel pore. Thus, keeping in mind that the distance between His37 and Val27 tetrads amounts to ∼16 Å, the molecular length for compound **1** of 5.9 Å (corrected by van der Waals radii of 2.0 and 1.7 for CH$_2$ and NH groups)[90,91] would span ∼9.6 Å, which would allow enough space for accommodating a chloride anion (ionic radius of 1.8 Å), covering a total length of 13.2 Å. This explains the significant reduction of the conformational heterogeneity of the Amt-bound M2 channel observed upon replacement of Amt by compound **1**. Likewise, it is reasonable to conceive that further extension of the ligand may lead to moderate enhancements in steric clashes with the side chains of Val27 residues, leading to the reduction in inhibitory potency observed for compounds **2** and **3**. On the other hand, it is worth noting that the stabilization afforded by the presence of the chloride anion would justify the pseudoirreversible inhibition observed for compound **2** in electrophysiological assays,[14] thus mimicking the behavior observed for Amt.

We hypothesize that compounds **1**, **3** and **4** should also exihibit a similar pseudoirreversible inhibition. To explore this

hypothesis, compound **4** was synthesized[18] and the kinetics of the inhibitory activity of **4** was tested on wt M2 channels expressed in *Xenopus laevis* oocytes, using the two-electrode voltage clamp (TEVC) technique.[63] The forward rate constant (k_{on}) for association of **4** was 2-fold lower compared to Amt (141 ± 6 and 293 ± 37 M^{-1} s^{-1} for **4** and Amt, respectively), presumably reflecting a slightly larger barrier for the adoption of the *down* arrangement, as expected from the enhanced volume of the pyrrolidine analogue. Noteworthy, at saturating compound concentration (100 μM), the reaction was found to be irreversible for **4** (Figure 9), an effect that may be attributed to the electrostatic trapping triggered by Cl$^-$ anions.
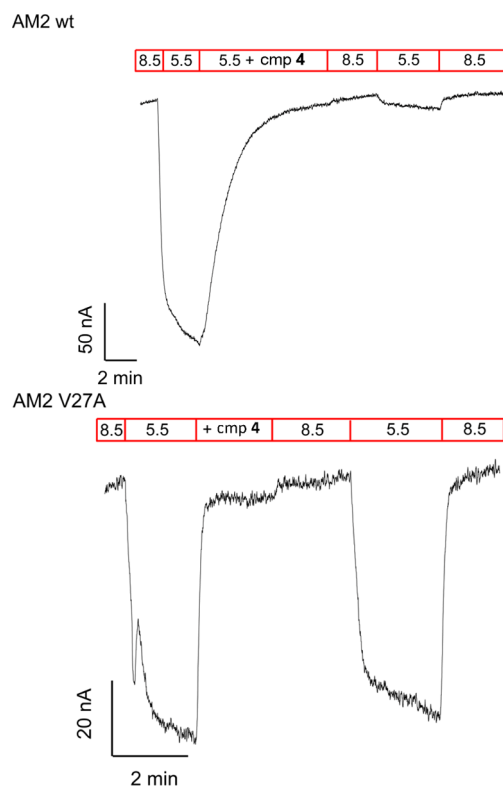

Figure 9. Inhibition of the A/M2 wt channel (derived from the A/Udorn/307/72 H3N2 virus strain) and V27A mutant form, using the TEVC technique in *Xenopus* oocytes. Oocytes were bathed in Barth's solution at pH = 8.5 and pH = 5.5. Current was clamped at −20 mV and compound **4** was applied at 100 μM in pH 5.5 solution once the inward current reached maximum amplitude in A/M2 wt channel (top) and V27A mutant channel (bottom).

The drastic loss of activity of Amt and **1** in the V27A channel is not unexpected keeping in mind both the enhanced size of the inner pore and the larger magnitude of the conformational fluctuations of the helices in the mutated channel, as noted in average volumes of 485 ± 64 and 601 ± 131 Å^3, respectively (as determined with Epock;[92] see Figures S8 and S9 in the Supporting Information). This should prevent the formation of strong interactions with the ligand, and the electrostatic repulsion with the protonated His37 residues would promote the adoption of the *up* arrangement, which was found to be the preferred binding mode of Amt in the unbiased MD simulations and in MW-WTM calculations (see above). In this case, it may be speculated that lengthening of the ligand does not suffice to restore the inhibitory potency, whereas increasing the volume of the hydrophobic cage leads effectively

to inhibition of the V27A channel (IC$_{50}$ values of 0.3 and 0.7 μM for **3** and **4**, respectively). Clearly, this geometrical change facilitates ligand desolvation, while enhancing the van der Waals interactions with the residues in the channel lumen, resulting in a tighter and more extended interaction as noted in ssNMR studies of **3** bound to the V27A variant.[15]

Since the presence of the chloride anion is significantly lowered in the mutated channel compared to the wt species (see above), we hypothesize that ligand binding would primarily involve the *up* binding mode. In this case, van der Waals forces would be the primary source to the binding affinity, and an enhanced size would afford an extended contact with the pore. However, as noted for Amt, this binding mode lacks an effective kinetic trapping, and the larger fluctuations of the V27A channel would facilitate release of the ligand upon washing at high pH in electrophysiological assays. Indeed, the current kinetics of the V27A channel was almost completely inhibited upon incubation with **4** (at 100 μM), but washing led to a recovery of the current kinetics, thus confirming the reversible nature of the binding (Figure 9). Overall, these experimental results support the validity of our computational model about the binding mechanism of Amt and Amt-related analogues to the wt M2 channel and its V27A variant.

■ CONCLUSION

This study allows us to suggest that (un)binding of Amt to the wt M2 channel is mediated by a sequential mechanism that involves the transient adoption of the *up* binding mode, followed by the rearrangement to the *down* state in the interior of the wt M2 channel. Access to the channel lumen is mainly driven by the hydrophobic interactions of the Amt cage with the side chains of Val27 residues, allowing Amt to adopt the *up* arrangement while attempting to preserve the interaction of the protonated amine with water molecules at the entrance of the channel. The *up* → *down* transition requires the flipping of Amt in the channel pore, a process that should a priori be hampered by the electrostatic repulsion between the positive charge of the protonated amine of Amt and the protonated rings of His37 residues. This transition is, however, facilitated by the presence of a chloride anion located between the tetrads formed by His37 and Trp41 residues, which would reduce the positive electrostatic potential in the interior of the channel, affording the electrostatic driving force for the Amt rearrangement and the adoption of the *down* state. At this point, it is worth noting that the presence of chloride anions has also been independently reported by other researchers,[66−68] using different simulation protocols and force fields, and has received experimental support from the finding of a chloride anion in the interior of the S31N mutated channel.[69] However, we also propose that the *down* binding mode is further stabilized by the presence of an additional chloride anion in the interior of the pore, leading to a double occupancy state with one chloride anion placed above the His37 tetrad and the other above the Trp41 one (see Figure 2), which would provide the electrostatic stabilization to trap Amt in the interior of the pore.

This mechanism permits to reconcile apparently contradictory experimental and theoretical results reported previously in the literature regarding the orientation of Amt in the channel pore, as present results demonstrate the ability of Amt to adopt both *up* and *down* orientations through a flipping mechanism within the pore of the channel.

Furthermore, we propose that chloride anions exert an active role in assisting the binding of Amt via kinetic trapping of the

ligand in the interior of the pore, which would contribute to the apparent tight binding reflected in the pseudoirreversible inhibition observed in electrophysiological assays. Thus, present results point out that the presence of chloride anions enhances the thermodynamic stability of the *down* binding mode by near 6 kcal/mol, leading to an overall stabilization of 12.1 kcal/mol and a net barrier of 18.7 kcal/mol for the release of Amt. Similar considerations can be expected to be involved in the binding of Amt analogues, as suggested for the pyrrolidine analogue **4**, which has an equipotent inhibitory activity compared to Amt (see Table 2). The trapping mechanism also provides an explanation to the pseudoirreversible binding reported previously for compound **2**. This effect reflects the mutually electrostatic intertwining between the protonated amine of these compounds and the chloride anions, a feature that should be taken into account in the design of novel antiviral compounds. Nevertheless, care must be taken in inferring a similar role of the chloride anions in assisting proton flux through the channel.

Finally, our results point out that the Val → Ala mutation has a dramatic effect on the free energy profile for Amt binding to the V27A channel (see Figure 6), thus providing an energetic basis to justify the dramatic reduction in the inhibitory activity of Amt in the mutated channel. The presence of chloride anions in the interior of the V27A variant is much less significant, and hence Amt adopts preferentially the *up* arrangement in the channel. In conjunction with the low dehydration of the ligand's protonated amine afforded by the wider pore originated upon the Val27 → Ala mutation, enhancement of the van der Waals interactions between ligand and the channel residues becomes the major driving force, which would not suffice to tighten the binding of the ligand, thus explaining the reversible inhibition observed experimentally. Taken together, this provides a rationale to understand the molecular basis of the drug resistance triggered by the Val → Ala mutation in the M2 channel, and opens new avenues in the design of M2 inhibitors.

ASSOCIATED CONTENT

S **Supporting Information**

The Supporting Information is available free of charge on the ACS Publications website at DOI: 10.1021/jacs.6b07096.

> Description of exploratory metadynamics, and selected results obtained from these simulations (PDF)

AUTHOR INFORMATION

Corresponding Authors

*andrea.cavalli@unibo.it
*fjluque@ub.edu

ORCID ^(iD)

Salomé Llabrés: 0000-0002-2039-7821
Jordi Juárez-Jiménez: 0000-0003-1464-1397
Matteo Masetti: 0000-0002-3757-7802
Santiago Vázquez: 0000-0002-9296-6026
F. Javier Luque: 0000-0002-8049-3567

Author Contributions

#S.L. and J.J.-J. have contributed equally to this work.

Notes

The authors declare no competing financial interest.

REFERENCES

(1) Chizhmakov, I. V.; Geraghty, F. M.; Ogden, D. C.; Hayhurst, A.; Antoniou, M.; Hay, A. J. *J. Physiol.* **1996**, *494*, 329−336.
(2) Pinto, L. H.; Lamb, R. A. *J. Biol. Chem.* **2006**, *281*, 8997−9000.
(3) Wei, C.; Pohorille, A. *Origins Life Evol. Biospheres* **2015**, *45*, 241−248.
(4) Wang, J.; Qiu, J. X.; Soto, C. S.; DeGrado, W. F. *Curr. Opin. Struct. Biol.* **2011**, *21*, 68−80.
(5) Takeda, M.; Pekosz, A.; Shuck, K.; Pinto, L. H.; Lamb, R. A. *J. Virol.* **2002**, *76*, 1391−1399.
(6) Samson, M.; Pizzorno, A.; Abed, Y.; Boivin, G. *Antiviral Res.* **2013**, *98*, 174−185.
(7) Wang, J.; Li, F.; Ma, C. *Biopolymers* **2015**, *104*, 291−309.
(8) Balannik, V.; Carnevale, V.; Fiorin, G.; Levine, B. G.; Lamb, R. A.; Klein, M. L.; DeGrado, W. F.; Pinto, L. H. *Biochemistry* **2010**, *49*, 696−708.
(9) Furuse, Y.; Suzuki, A.; Kamigaki, T.; Oshitani, H. *Virol. J.* **2009**, *6*, 67.
(10) Hu, W.; Zeng, S.; Li, C.; Jie, Y.; Li, Z.; Chen, L. *J. Med. Chem.* **2010**, *53*, 3831−3834.
(11) Zhao, X.; Jie, Y.; Rosenberg, M. R.; Wan, J.; Zeng, S.; Cui, W.; Xiao, Y.; Li, Z.; Tu, Z.; Casarotto, M. G.; Hu, W. *Antiviral Res.* **2012**, *96*, 91−99.
(12) Zhao, X.; Zhang, Z.-W.; Cui, W.; Chen, S.; Zhou, Y.; Dong, J.; Jie, Y.; Wan, J.; Xu, Y.; Hu, W. *MedChemComm* **2015**, *6*, 727−731.
(13) Wu, S.; Huang, J.; Gazzarrini, S.; He, S.; Chen, L.; Li, J.; Xing, L.; Li, C.; Chen, L.; Neochoritis, C. G.; Liao, G. P.; Zhou, H.; Dömling, A.; Moroni, A.; Wang, W. *ChemMedChem* **2015**, *10*, 1837−1845.
(14) Balannik, V.; Wang, J.; Ohigashi, Y.; Jing, X.; Magavern, E.; Lamb, R. A.; DeGrado, W. F.; Pinto, L. H. *Biochemistry* **2009**, *48*, 11872−11882.
(15) Wang, J.; Ma, C.; Fiorin, G.; Carnevale, V.; Wang, T.; Hu, F.; Lamb, R. A.; Pinto, L. H.; Hong, M.; Klein, M. L.; DeGrado, W. F. *J. Am. Chem. Soc.* **2011**, *133*, 12834−12841.
(16) Wang, J.; Ma, C.; Wu, Y.; Lamb, R. A.; Pinto, L. H.; DeGrado, W. F. *J. Am. Chem. Soc.* **2011**, *133*, 13844−13847.
(17) Rey-Carrizo, M.; Torres, E.; Ma, C.; Barniol-Xicota, M.; Wang, J.; Wu, Y.; Naesens, L.; DeGrado, W. F.; Lamb, R. A.; Pinto, L. H.; Vázquez, S. *J. Med. Chem.* **2013**, *56*, 9265−9274.
(18) Rey-Carrizo, M.; Barniol-Xicota, M.; Ma, C.; Frigolé-Vivas, M.; Torres, E.; Naesens, L.; Llabrés, S.; Juárez-Jiménez, J.; Luque, F. J.; DeGrado, W. F.; Lamb, R. A.; Pinto, L. H.; Vázquez, S. *J. Med. Chem.* **2014**, *57*, 5738−5747.
(19) Wu, Y.; Canturk, B.; Jo, H.; Ma, C.; Gianti, E.; Klein, M. L.; Pinto, L. H.; Lamb, R. A.; Fiorin, G.; Wang, J.; DeGrado, W. F. *J. Am. Chem. Soc.* **2014**, *136*, 17987−17995.
(20) Li, F.; Ma, C.; DeGrado, W. F.; Wang, J. *J. Med. Chem.* **2016**, *59*, 1207−1216.
(21) Acharya, R.; Carnevale, V.; Fiorin, G.; Levine, B. G.; Polishchuk, A. L.; Balannik, V.; Samish, I.; Lamb, R. A.; Pinto, L. H.; DeGrado, W. F.; Klein, M. L. *Proc. Natl. Acad. Sci. U. S. A.* **2010**, *107*, 15075−15080.

(22) Stouffer, A. L.; Acharya, R.; Salom, D.; Levine, A. S.; Di Costanzo, L.; Soto, C. S.; Tereshko, V.; Nanda, V.; Stayrook, S.; DeGrado, W. F. *Nature* **2008**, *451*, 596−599.

(23) Thomaston, J. L.; Alfonso-Prieto, M.; Woldeyes, R. A.; Fraser, J. S.; Klein, M. L.; Fiorin, G.; DeGrado, W. F. *Proc. Natl. Acad. Sci. U. S. A.* **2015**, *112*, 14260−14265.

(24) Schnell, J. R.; Chou, J. J. *Nature* **2008**, *451*, 591−595.

(25) Cady, S. D.; Mishanina, T. V.; Hong, M. *J. Mol. Biol.* **2009**, *385*, 1127−1141.

(26) Cady, S. D.; Schmidt-Rohr, K.; Wang, J.; Soto, C. S.; DeGrado, W. F.; Hong, M. *Nature* **2010**, *463*, 689−692.

(27) Sharma, M.; Yi, M.; Dong, H.; Qin, H.; Peterson, E.; Busath, D. D.; Zhou, H.-X.; Cross, T. A. *Science* **2010**, *330*, 509−512.

(28) Miao, Y.; Qin, H.; Fu, R.; Sharma, M.; Can, T. V.; Hung, I.; Luca, S.; Gor'kov, P. L.; Brey, W. W.; Cross, T. A. *Angew. Chem., Int. Ed.* **2012**, *51*, 8383−8386.

(29) Pielak, R. M.; Chou, J. J. *Biochem. Biophys. Res. Commun.* **2010**, *401*, 58−63.

(30) Andreas, L. B.; Eddy, M. T.; Chou, J. J.; Griffin, R. G. *J. Am. Chem. Soc.* **2012**, *134*, 7215−7218.

(31) Wang, J.; Wu, Y.; Ma, C.; Fioriin, G.; Wang, J.; Pinto, L. H.; Lamb, R. A.; Klein, M. L.; DeGrado, W. L. *Proc. Natl. Acad. Sci. U. S. A.* **2013**, *110*, 1315−1320.

(32) Andreas, L. B.; Reese, M.; Eddy, M. T.; Gelev, V.; Ni, Q. Z.; Miller, E. A.; Emsley, L.; Pintacuda, G.; Chou, J. J.; Griffin, R. G. *J. Am. Chem. Soc.* **2015**, *137*, 14877−14886.

(33) Andreas, L. B.; Barnes, A. B.; Corzilius, B.; Chou, J. J.; Miller, E. A.; Caporini, M.; Rosay, M.; Griffin, R. G. *Biochemistry* **2013**, *52*, 2774−2782.

(34) Wright, A. K.; Batsomboon, P.; Dai, J.; Hung, I.; Zhou, H.-X.; Dudley, G. B.; Cross, T. A. *J. Am. Chem. Soc.* **2016**, *138*, 1506−1509.

(35) Lomize, M. A.; Lomize, A. L.; Pogozheva, I. D.; Mosberg, H. I. *Bioinformatics* **2006**, *22*, 623−625.

(36) Jo, S.; Kim, T.; Iyer, V. G.; Im, W. *J. Comput. Chem.* **2008**, *29*, 1859−1865.

(37) Jo, S.; Lim, J. B.; Klauda, J. B.; Im, W. *Biophys. J.* **2009**, *97*, 50−58.

(38) Jorgensen, W. L.; Chandrasekhar, J.; Madura, J. D.; Impey, R. W.; Klein, M. L. *J. Chem. Phys.* **1983**, *79*, 926.

(39) Hornak, V.; Abel, R.; Okur, A.; Strockbine, B.; Roitberg, A.; Simmerling, C. *Proteins: Struct., Funct., Genet.* **2006**, *65*, 712−725.

(40) Wang, J.; Wolf, R. M.; Caldwell, J. W.; Kollman, P. A.; Case, D. A. *J. Comput. Chem.* **2004**, *25*, 1157−1174.

(41) Wang, J.; Cieplak, P.; Kollman, P. A. *J. Comput. Chem.* **2000**, *21*, 1049−1074.

(42) Case, D. A.; Darden, T. A.; Cheatham, T. E.; Simmerling, C. L.; Wang, J.; Duke, R. E.; Luo, R.; Walker, R. C.; Zhang, W.; Merz, K. M.; Roberts, B.; Hayik, S.; Roitberg, A.; Seabra, G.; Swails, J.; Goetz, A. W.; Kolossváry, I.; Wong, K. F.; Paesani, F.; Vanicek, J.; Wolf, R. M.; Liu, J.; Wu, X.; Brozell, S. R.; Steinbrecher, T.; Gohlke, H.; Cai, Q.; Ye, X.; Wang, J.; Hsieh, M. J.; Cui, G.; Roe, D. R.; Mathews, D. H.; Seetin, M. G.; Salomon-Ferrer, R.; Sagui, C.; Babin, V.; Luchko, T.; Gusarov, S.; Kovalenko, A.; Kollman, P. A. *AMBER 12*; 2012.

(43) Dickson, C. J.; Rosso, L.; Betz, R. M.; Walker, R. C.; Gould, I. R. *Soft Matter* **2012**, *8*, 9617−9627.

(44) Joung, I. S.; Cheatham, T. E. *J. Phys. Chem. B* **2008**, *112*, 9020−9041.

(45) Hu, J.; Fu, R.; Nishimura, K.; Zhang, L.; Zhou, H. X.; Busath, D. D.; Vijayvergiya, V.; Cross, T. A. *Proc. Natl. Acad. Sci. U. S. A.* **2006**, *103*, 6865−6870.

(46) Hu, F.; Schmidt-Rohr, K.; Hong, M. *J. Am. Chem. Soc.* **2011**, *134*, 3703−3713.

(47) Colvin, M. T.; Andreas, L. B.; Chou, J. J.; Griffin, R. G. *Biochemistry* **2014**, *53*, 5987−5994.

(48) Miao, Y.; Fu, R.; Zhou, H.-X.; Cross, T. *Structure* **2015**, *23*, 2300−2308.

(49) Liao, S. Y.; Yang, Y.; Tietze, D.; Hong, M. *J. Am. Chem. Soc.* **2015**, *137*, 6067−6077.

(50) Williams, J. K.; Tietze, D.; Lee, M.; Wang, J.; Hong, M. *J. Am. Chem. Soc.* **2016**, *138*, 8143−8155.

(51) Rey-Carrizo, M.; Gazzarrini, S.; Llabrés, S.; Frigolé-Vivas, M.; Juárez-Jiménez, J.; Font-Bardia, M.; Naesens, L.; Moroni, A.; Luque, F. J.; Vázquez, S. *Eur. J. Med. Chem.* **2015**, *96*, 318−329.

(52) Phillips, J. C.; Braun, R.; Wang, W.; Gumbart, J.; Tajkhorshid, E.; Villa, E.; Chipot, C.; Skeel, R. D.; Kalé, L.; Schulten, K. *J. Comput. Chem.* **2005**, *26*, 1781−1802.

(53) Ryckaert, J.-P.; Ciccotti, G.; Berendsen, H. J. C. *J. Comput. Phys.* **1977**, *23*, 327−341.

(54) Darden, T.; York, D.; Pedersen, L. *J. Chem. Phys.* **1993**, *98*, 10089.

(55) Baker, N. A.; Sept, D.; Joseph, S.; Holst, M. J.; McCammon, J. A. *Proc. Natl. Acad. Sci. U. S. A.* **2001**, *98*, 10037−10041.

(56) Laio, A.; Parrinello, M. *Proc. Natl. Acad. Sci. U. S. A.* **2002**, *99*, 12562−12566.

(57) Cavalli, A.; Spitaleri, A.; Saladino, G.; Gervasio, F. L. *Acc. Chem. Res.* **2015**, *48*, 277−285.

(58) De Vivo, M.; Massetti, M.; Bottegoni, G.; Cavalli, A. *J. Med. Chem.* **2016**, *59*, 4035−4061.

(59) Bonomi, M.; Branduardi, D.; Bussi, G.; Camilloni, C.; Provasi, D.; Raiteri, P.; Donadio, D.; Marinelli, F.; Pietrucci, F.; Broglia, R. A.; Parrinello, M. *Comput. Phys. Commun.* **2009**, *180*, 1961.

(60) Tribello, G. A.; Bonomi, M.; Branduardi, D.; Camilloni, C.; Bussi, G. *Comput. Phys. Commun.* **2014**, *185*, 604−613.

(61) Barducci, A.; Bussi, G.; Parrinello, M. *Phys. Rev. Lett.* **2008**, *100*, 020603.

(62) Raiteri, P.; Laio, A.; Gervasio, F. L.; Micheletti, C.; Parrinello, M. *J. Phys. Chem. B* **2006**, *110*, 3533−3539.

(63) Gazzarrini, S.; Kang, M.; Abenavoli, A.; Romani, G.; Olivari, G.; Gaslini, D.; Ferrara, G.; Van Etten, J. L.; Kreim, M.; Kast, S. M.; Thiel, G.; Moroni, A. *Biochem. J.* **2009**, *420*, 295−303.

(64) Gu, R.-X.; Liu, L. A.; Wang, Y.-H.; Xu, Q.; Wei, D.-Q. *J. Phys. Chem. B* **2013**, *117*, 6042−6051.

(65) Wilman, H. R.; Shi, J.; Deane, C. M. *Proteins: Struct., Funct., Genet.* **2014**, *89*, 1960−1970.

(66) Mustafa, M.; Henderson, D. J.; Busath, D. D. *Proteins: Struct., Funct., Genet.* **2009**, *76*, 794−807.

(67) Wei, C.; Pohorille, A. *Biophys. J.* **2013**, *105*, 2036−2045.

(68) Gkeka, P.; Eleftheratos, S.; Kolocouris, A.; Cournia, Z. *J. Chem. Theory Comput.* **2013**, *9*, 1272−1281.

(69) Thomaston, J. L.; DeGrado, W. F. *Protein Sci.* **2016**, *25*, 1551−1554.

(70) Leonov, H.; Astahan, P.; Krugliak, M.; Arkin, I. T. *J. Am. Chem. Soc.* **2011**, *133*, 9903−9911.

(71) Alhadeff, R.; Assa, D.; Astahan, P.; Krugliak, M.; Arkin, I. T. *Biochim. Biophys. Acta, Biomembr.* **2014**, *1838*, 1068−1073.

(72) Ma, C.; Polishchuk, A. L.; Ohigashi, Y.; Stouffer, A. L.; Schön, A.; Magavern, E.; Jing, X.; Lear, J. D.; Freire, E.; Lamb, R. A.; DeGrado, W. F.; Pinto, L. H. *Proc. Natl. Acad. Sci. U. S. A.* **2009**, *106*, 12283.

(73) Gleed, M. L.; Ioannidis, H.; Kolocouris, A.; Busath, D. D. *J. Phys. Chem. B* **2015**, *119*, 11548−11559.

(74) Gleed, M. L.; Busath, D. D. *J. Phys. Chem. B* **2015**, *119*, 1225−1231.

(75) Khurana, E.; DeVane, R. H.; Dal Peraro, M.; Klein, M. L. *Biochim. Biophys. Acta, Biomembr.* **2011**, *1808*, 530−537.

(76) Saotome, K.; Duong-Ly, K. C.; Howard, K. P. *Biopolymers* **2015**, *104*, 405−411.

(77) Wang, C.; Takeuchi, K.; Pinto, L. H.; Lamb, R. A. *J. Virol.* **1993**, *67*, 5585−5594.

(78) Rosenberg, M. R.; Casarotto, M. G. *Proc. Natl. Acad. Sci. U. S. A.* **2010**, *31*, 13866−13871.

(79) Horovitz, A.; Serrano, L.; Avron, B.; Bycroft, M.; Fersht, A. *J. Mol. Biol.* **1990**, *216*, 1031−1044.

(80) Sali, D.; Bycroft, M.; Fersht, A. R. *J. Mol. Biol.* **1991**, *220*, 779−788.

(81) Dao-Pin, S.; Sauer, U.; Nicholson, H.; Matthews, B. W. *Biochemistry* **1991**, *30*, 7142−7153.

(82) Waldburger, C. D.; Schildbach, J. F.; Sauer, R. T. *Nat. Struct. Biol.* **1995**, *2*, 122−128.

(83) Hendsch, Z. S.; Tidor, B. *Protein Sci.* **1994**, *3*, 211−226.

(84) Sharma, M.; Li, C.; Busath, D. D.; Zhou, H. X.; Cross, T. A. *Biochim. Biophys. Acta, Biomembr.* **2011**, *1808*, 538−546.

(85) Stouffer, A. L.; Ma, C.; Cristian, L.; Ohigashi, Y.; Lamb, R. A.; Lear, J. D.; Pinto, L. H.; DeGrado, W. F. *Structure* **2008**, *16*, 1067−1076.

(86) Homeyer, N.; Ioannidis, H.; Kolarov, F.; Gauglitz, G.; Zikos, C.; Kolocouris, A.; Gohlke, H. *J. Chem. Inf. Model.* **2016**, *56*, 110−126.

(87) Ioannidis, H.; Drakopoulos, A.; Tzitzoglaki, C.; Homeyer, N.; Kolarov, F.; Paraskevi, G.; Freudenberger, K.; Liolios, C.; Gauglitz, G.; Cournia, Z.; Gohlke, H.; Kolocouris, A. *J. Chem. Inf. Model.* **2016**, *56*, 862−876.

(88) Du, J.; Cross, T. A.; Zhou, H.-X. *Drug Discovery Today* **2012**, *17*, 1111−1120.

(89) Wang, J.; Cady, S. D.; Balannik, V.; Pinto, L. H.; DeGrado, W. F.; Hong, M. *J. Am. Chem. Soc.* **2009**, *131*, 8066−8076.

(90) Kammeyer, C. W.; Whitman, D. R. *J. Chem. Phys.* **1972**, *56*, 4419−4421.

(91) Pauling, L. *The Nature of the Chemical Bond*; Cornell U. P.: Ithaca, NY, 1960; p 260.

(92) Laurent, B.; Chavent, M.; Cragnolini, T.; Dahl, A. C.; Pasquali, S.; Derremaux, P.; Sansom, M. S.; Baaden, M. *Bioinformatics* **2015**, *31*, 1478−1480.

(93) *Molecular Operating Environment (MOE)*, 2013.08; Chemical Computing Group Inc.: Montreal, QC, 2016.